Analysis of the Secondary Structure of Random Copolymers by a Combination of Fluorescence and Molecular Dynamics Methods. Application to Polyphosphazenes Containing Phenoxy and Binaphthoxy Groups

Gema Marcelo,[†] Enrique Saiz,*[,†] Francisco Mendicuti,[†] Gabino A. Carriedo,[‡] Francisco J. García Alonso,[‡] and Jose L. García Alvarez[‡]

Departamento de Química Física, Universidad de Alcalá, 28871 Alcalá de Henares, Madrid, Spain, and Departamento de Química Orgánica e Inorgánica, Facultad de Química, Universidad de Oviedo, Oviedo 33071, Spain

Received September 22, 2005; Revised Manuscript Received November 9, 2005

ABSTRACT: Steady-state and time-resolved fluorescence techniques are combined with theoretical molecular dynamics calculations and applied to study the secondary structure of some random copolymers of polyphophazenes containing phenoxy and binaphthoxy chromophoric groups. Analysis of excitation and emission spectra, fluorescence depolarization and lifetimes suggested that 100% of the excitation energy of the phenoxy groups is transferred to the binaphthoxy groups. Subsequently, this energy migrates among binaphthoxy groups along the polymer chain. This migration produces a noticeable quenching of the binaphthoxy fluorescence. The efficiency of this energy migration process increases with two features of the copolymer chain, namely, the fraction of binaphthoxy groups and the presence of helical sequences along the chain. Molecular dynamics simulations on several polymer fragments were used to obtain parameters related to the allowed energy-transfer processes. The results of these simulations are in good agreement with the conclusions obtained from the experimental measurements.

Introduction

Polyphosphazenes are a kind of greatly varied performance organic/inorganic polymers containing a highly flexible inorganic phosphorus−nitrogen backbone. The appropriate selection of substituents at the phosphorus allows control of many polymer properties over a much broader range than is possible with most other polymer systems.[1−3] Attachment of chiral groups to the polymer chain may produce optically active chiral macromolecules of great interest to modern chemistry. In fact, it has been demonstrated that the incorporation of chiral 1,1′-binaphthoxy groups into the main polyphosphazene chain yields optically active materials.[4,5] Nevertheless, the analysis of the specific rotation of these polymeric phosphazenes also infers the induction of an additional macromolecular asymmetry due to the formation of a helicoidal secondary structures along the chain.

In this sense the synthesis, characterization, and analysis of some solution properties of optically active polyphosphazenes, *R*-(−)- and *S*-(+)-$[NP(O_2C_{20}H_{12})]_n$ homopolymers and random copolymers of general formulas $\{[NP(O_2C_{20}H_{12})]_x[NP(OC_6H_5)_2]_{1-x}\}_n$ containing both binaphthoxy ($O_2C_{20}H_{12}$) and phenoxy (OC_6H_5) groups with different molar composition *x* have been reported earlier.[4,5] When these homopolymers dissolve in good solvents, they behave like random coils with high values of the characteristic ratio which suggest a rather strong preference for extended conformations. The specific rotation and its dependence on molecular weight seem to indicate the presence of a secondary helicoidal structure that should contribute to the optical rotation values and the large unperturbed dimensions. Most of these copolymers aggregate in a globular shape or are in a random coil, and the specific rotation tends to increase with the number of binaphthoxy units. These results may agree with the presence of helicoidal segments placed locally along the chain whose contribution to the specific rotation increases with *x*.

On the other hand, molecular dynamics simulations performed on poly(biphenoxy)-[6] and poly(binaphthoxy)phosphazene homopolymers[7] also predicted the possibility of conformations in those chains capable of producing fragments containing short helices. Large-angle X-ray scattering measurements on the *R*-(−)-$[NP(O_2C_{20}H_{12})]_n$ homopolymer in the solid amorphous state also reveal this helicity.[7] It has recently been reported that the thermal degradation of isotactic *R*-(−)-$[NP(O_2C_{20}H_{12})]_n$ to lower M_w distributions is accompanied by a significant decrease in the specific rotation in solution.[8] The strong and reversible variation of the specific rotation with the temperature and the dependence on the wavelength for this system also supports the presence of a secondary helicoidal structure. On the contrary, the specific rotation of the related random nonisotactic copolymer (*R*/*S*)-$[NP(O_2C_{20}H_{12})]_n$, having different proportions of the chiral *R* and *S* repeating units, consistently did not depend on M_w and the temperature.

As these polymers contain binaphthoxy chromophore groups, we also reported some fluorescence measurements in various solvents and temperatures.[8] Intramolecular excimer formation, which has a conformational origin, might be sensitive to the presence of helicoidal segments placed along the chain. Unfortunately, none of the polymers studied so far showed intramolecular excimers. These measurements neither support nor exclude the existence of the helicoidal fragments.

In this work we use several fluorescence techniques on dilute solution of *R*-(−)-, *S*-(+)-$[NP(O_2C_{20}H_{12})]_n$, and *R*/*S*-$[NP(O_2C_{20}H_{12})]_n$ (optically inactive 0.5-*R*/*S*) homopolymers, as well

* Corresponding author: Ph 34-91-8854672; Fax 34-91-8854763; e-mail Enrique.saiz@uah.es.
[†] Universidad de Alcalá.
[‡] Universidad de Oviedo.

10.1021/ma052063d CCC: $33.50 © 2006 American Chemical Society
Published on Web 12/24/2005

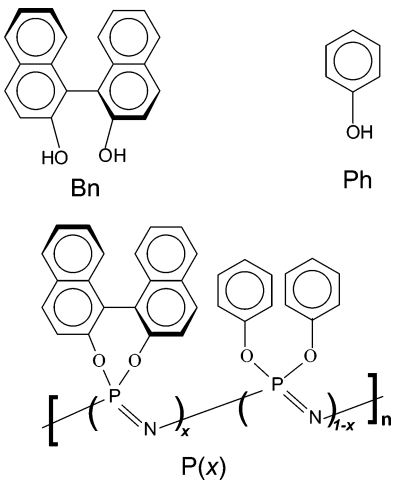

Figure 1. Structures for $\{[NP(O_2C_{20}H_{12})]_x[NP(OC_6H_5)_2]_{1-x}\}_n$, P(*x*), and *R*-(+)-1,1′-binaphthyl-2,2′diol (Bn) and phenol (Ph) model compounds.

as six random copolymers $\{[NP(O_2C_{20}H_{12})]_x[NP(OC_6H_5)_2]_{1-x}\}_n$ with different composition *x*, to study the photophysical behavior of these systems. Special emphasis is placed on studying the intramolecular energy transfer by a resonance mechanism[9] where binaphthoxy and phenoxy chromophores are involved. Intramolecular energy transfer efficiency, which also depends on the polymer conformation,[10,11] may also provide information on the secondary structure in solution of these polymers. Molecular dynamics (MD)[12,13] is also employed to simulate several oligomers and to calculate several parameters related to the efficiency of the energy-transfer processes that may occur in these systems.

Experimental Section

Materials. Optically inactive racemic polymer *R*/*S*-$[NP(O_2C_{20}H_{12})]_n$ (0.5-*R*/*S* binaphthoxyphosphazene, $\alpha = 0$, $M_w = 0.8 \times 10^6$, $M_w/M_n = 4.0$, and chlorine content = 0.19%) and optically active *R*-(−)-$[NP(O_2C_{20}H_{12})]_n$ ($\alpha = -192$, $M_w = 0.84 \times 10^6$, $M_w/M_n = 2.5$, and Cl (%) = 0.39) and *S*-(+)-$[NP(O_2C_{20}H_{12})]_n$ ($\alpha = +209$, $M_w = 1.1 \times 10^6$, $M_w/M_n = 3.6$, and Cl (%) = 0.1) were prepared as described elsewhere;[4,8] commercially available homopolymer $[NP(OC_6H_5)_2]_n$ (phenoxyphosphazene, $M_w = 2.0 \times 10^6$, $M_w/M_n = 2.0$) was purchased from Aldrich and purified by precipitation in *n*-hexane from tetrahydrofuran. Six random copolymers $\{[NP(O_2C_{20}H_{12})]_x[NP(OC_6H_5)_2]_{1-x}\}_n$, whose structure is depicted in Figure 1, where *x* is the molar fraction content of R-binaphthoxy groups, were synthesized as described in a previous work.[5] Copolymers have weight-average molecular weights M_w and M_w/M_n ranging from 0.93×10^6 up to 1.2×10^6 and from 1.9 to 4.6, respectively. Unsubstituted chlorine content was always smaller than 0.1%. In the remainder of the paper homopolymers and random copolymers will be identified as P(*x*), i.e., P(0), P(0.08), P(0.17), P(0.23), P(0.32), P(0.42), P(0.70), and P(1). With regard to the $[NP(O_2C_{20}H_{12})]_n$ homopolymers described at the beginning of this paragraph, they will be distinguished as *R*/*S*-P(1), *R*-P(1), and *S*-P(1). The *R*-(+)-1,1′-binaphthyl-2,2′diol (*R*-binaphthol) (Aldrich, 99% ee/HPLC) and phenol (Aldrich, 99%), denoted Bn and Ph, respectively, were used as model compounds without any further purification. The solvents 1,2-dichloroethane (DCE, +99%), tetrahydrofuran (THF, spectrophotometric grade), and 1-methyl-2-pyrrolidinone (NMP, spectrophotometric grade) were purchased from Aldrich, and they were used without further purification.

Instrumentation and Methods. Steady-state fluorescence measurements were performed on an SLM 8100 Aminco spectrofluorimeter equipped with a Xe lamp, a double (single) concave grating monochromator at the excitation (emission) path, and Glan-Thompson prism polarizers in both paths. The photomultiplier was cooled by a Peltier system. The excitation and emission slit widths were set to 8 nm.

Fluorescence decay measurements were obtained on a TCSPC FL900 Edinburgh Instruments spectrometer by using a thyratron-gated lamp filled with H_2 and equipped with two concave grating monochromators at both the excitation and emission paths and a red sensitive photomultiplier immersed in a Peltier-cooled housing. Slits were set to a bandwidth of 18 nm. The data acquisition was carried out by using 1024 channels and a time window width of 100 ns with a total of 10 000 counts at the maximum peak of intensity. The instrumental response function was regularly obtained by measuring the scattering of a Ludox solution. Decay intensity profiles were fitted to a sum of exponential decay functions as

$$I(t) = \sum_{i=1}^{n} B_i e^{-t/\tau_i} \tag{1}$$

by the iterative reconvolution method.[14] The average lifetime of a multiple-exponential decay function was then defined as

$$\langle \tau \rangle = \frac{\sum_1^n B_i \tau_i^2}{\sum_1^n B_i \tau_i} \tag{2}$$

where B_i is the preexponential factor of the component with a lifetime τ_i of the multiexponential function intensity decay.

Right angle geometry and rectangular 10 mm path cells were used for all fluorescence dilute solution measurements. In addition, magic angle conditions were used for the steady-state measurements with the obvious exception of fluorescence polarization ones. Absorbances of these samples at the wavelength of excitation (mainly 270 and 305 nm) were approximately in the 0.1−0.2 interval. The polymer concentration for these solutions was very small, thus avoiding the possible intermolecular interactions and inner filter effects. Solvent baselines were measured and subtracted from the spectra when fluorescence signals were low.

The fluorescence depolarization measurements for the samples in solution were obtained by the well-known "single-channel or L-format" method.[15] Thus, the anisotropy *r* was defined as

$$r = (I_{VV} - GI_{VH})/(I_{VV} + 2GI_{VH}) \tag{3}$$

where I_{xy} is the intensity of the emission that is measured when the excitation polarizer is in position *x* (V for vertical, H for horizontal), the emission polarizer is in position *y*, and the *G* factor ($= I_{HV}/I_{HH}$) corrects for any depolarization produced by the optical system.

The Förster radius R_0 for a resonance energy transfer donor (D) to acceptor (A) process[9] was defined by[16−18]

$$R_0^6 = 9000 \ln 10\, \kappa^2 \phi_D J/125\pi^5 n^4 N_a \tag{4}$$

where ϕ_D denotes the fluorescence quantum yield of D in the absence of A, *n* is the refractive index of the medium, κ^2 is the orientational factor, and N_a is Avogadro's number. This equation is also valid when D and A are the same species that self-transfer the energy. *J* is the overlap integral between the normalized fluorescence intensity, $I(\lambda)$, and the absorption spectrum, $\epsilon(\lambda)$, of such species defined as

$$J = \int \lambda^4 I(\lambda)\, \epsilon(\lambda)\, d\lambda \tag{5}$$

Molecular Dynamics (MD) Details

MD trajectories were computed for four isolated oligomers which reproduce different portions of the polymers experimentally studied. The DL_POLY package[19] and the Amber force field,[20] including some parameters for polyphosphazenes used previously,[21,22] were employed. Three of the fragments consisted

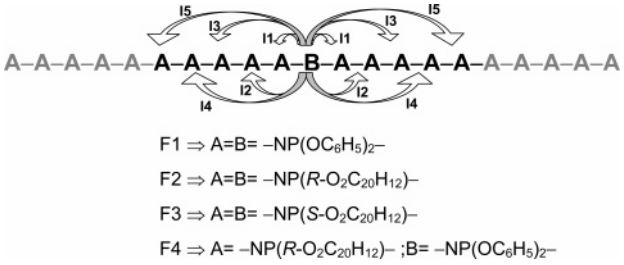

Figure 2. Scheme of F1−F4 fragments simulated by MD and interaction types I1−I5.

of 21 phosphazene repeating units, $A_{10}-B-A_{10}$, where A and B were the following entities: A = B = $-NP(OC_6H_5)_2-$; A = B = $-NP(R-O_2C_{20}H_{12})-$, and A = B = $-NP(S-O_2C_{20}H_{12})-$. These structures (Figure 2) simulate the phenoxyphosphazene and the optically active *R*- and *S*-binaphthoxyphosphazene homopolymers, respectively. The fourth fragment studied corresponds to A= $-NP(R-O_2C_{20}H_{12})-$ and B = $-NP(OC_6H_5)_2-$. They will be identified as F1, F2, F3, and F4, respectively. C−H bond lengths were kept constant during the simulations by means of the SHAKE algorithm.[13] All other bond lengths, bond angles, and torsion angles were variable during the simulations. The total potential energy of each fragment was considered as the sum of bond stretching, angle bending, intrinsic rotational barriers, van der Waals interactions, and Coulombic energies. A relative permittivity function of the interatomic distance *r* ($\epsilon = \epsilon_0 r$) was used for the electrostatic interactions. The Sybyl package[23] was used for constructing the fragments studied. Partial charges assigned to every atom were obtained by the Gasteiger−Hückel method,[24,25] which is included in the same package.[23] Results, however, reveal that the electrostatic interactions are not very important, and they do not change much with the charge distribution used. The simulations were started on optimized helical conformations of F1−F4 fragments, whose potential energy was minimized by using a simplex algorithm followed by a conjugate gradient procedure.[23,26,27] Each simulation was performed beginning with a warming equilibration period during which the temperature was increased from 0 K to the temperature of interest at 15 K intervals. The structures were kept at each of these temperatures for 5 ps. After this period a trajectory of 1 ns (10^6 fs) was completed. A time step of 1 fs for the integration equations of motion was used. The temperature of the system was maintained constant by means of a Nose−Hoover thermostat[13] with a relaxation time of 500 fs. Cutoff distances of 9.6 and 8 Å were used for Coulombic and van der Waals interactions, respectively. Coordinates of relevant atoms were saved at intervals of 1 ps for subsequent analysis, which means a total of 1000 conformations for each fragment. The average of any property was calculated by equally weighing each of these conformations.

The quality of the statistical sampling over the conformational space was initially analyzed by studying the evolution over time of the rotational angles around the skeletal bonds and the interatomic distances between some pairs of atoms within the molecules from MD trajectories at several temperatures (300−1000 K). The results indicate that at 300 K the atomic mobility is far too small to allow the passage over the potential energy barriers separating adjacent conformational minima. At 500 K the energy barriers can be surmounted, but the passage from one conformation to another is very slow; consequently, the sampling within a 1 ns MD trajectory is rather poor. All the results presented below were obtained at 1000 K, which provides an excellent sampling. However, it should be pointed out that the results are practically identical to those computed at 750 K.

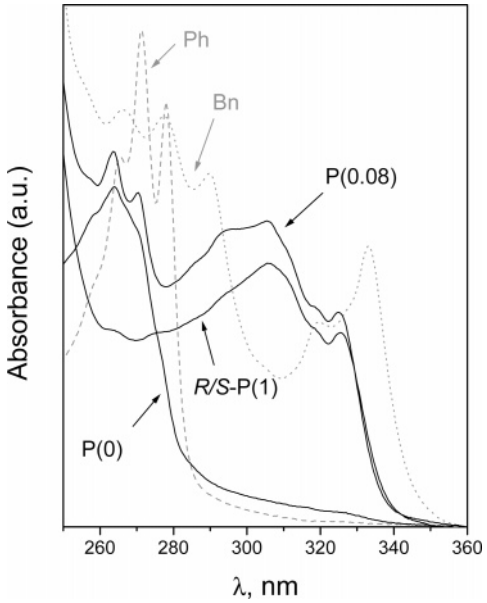

Figure 3. Absorption spectra for dilute solutions of *R*/*S*-P(1), P(0), and P(0.08) polymers and the Bn and Ph model compounds (dashed lines) in DCE at 25 °C.

Results and Discussion

Absorption Spectra. As depicted in Figure 3, Ph exhibits one main band with three maxima placed at approximately 265, 272, and 278 nm. Bn, however, shows two main bands with peaks centered at 266, 278, and 290 nm and 320 and 332 nm. P(0) displays a spectrum similar to that of Ph but is slightly shifted to the high region by about ∼8 nm, showing a peak at 264 nm and two shoulders around 258 and 270 nm. R/S−P(1) shows a distinguishable main band with a maximum placed at 305 nm and shoulders at 292 nm and 320 and 325 nm. P(0.08) and other copolymers display a combination of bands coming from the spectra for P(0) and (P1). The high-energy band intensity relative to the low-energy one decreases with the molar fraction of binaphthoxy groups (BnO), *x*. Spectra in THF and NMP show similar characteristics.

Emission Spectra. Emission spectra for P(*x*) and model compounds were obtained upon excitation of 270 and 305 nm (325 nm for Bn), the direct excitation of phenoxy (PhO) and binaphthoxy groups (BnO), respectively. Nevertheless, BnO also absorbs at 270 nm. As shown in Figure 4, the spectrum for Ph reveals a single band centered at ∼292 nm, which is typical of the benzene group. P(0) shows a broadening to the red of the monomer band observed for Ph, which is attributed to the emission of intramolecular excimers.[28] Excimer emission intensity depends on the nature of the solvent used. The Bn model compound exhibits a single band whose maximum is located around 355−360 nm and a shoulder at ∼380 nm. The homopolymer *R*/*S*-P(1) does not, however, show any broadening that could indicate the presence of intramolecular excimers by sandwich-type overlapping of a pair of BnO. The lack of these excimers, just as with biphenyl excimers in homogeneous solutions,[29] was attributed to the nonstability of such excimers which is probably due to the spacial arrangement of both naphthalenes in BnO.[8] Spectra for P(0.08), the copolymer with the highest PhO content (near 90%), and the other copolymers when excited at 270 or 305 nm only display the emission of BnO. This indicates a 100% efficient PhO → BnO energy transfer, whichever the value of *x* and whatever the solvent (THF, DCE, or NMP) used.

Excitation Spectra. Placement (not intensity) of relevant bands of different compounds (Figure 5) observed in excitation

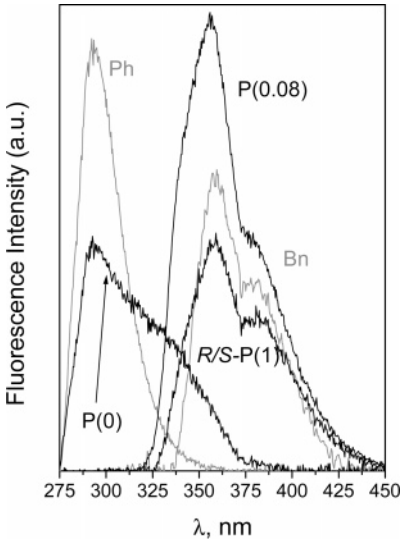

Figure 4. Uncorrected emission spectra for dilute solutions of Ph, Bn, P(0), P(0.08), and *R*/*S*-P(1) in DCE at 25 °C upon excitation wavelength of 270 nm.

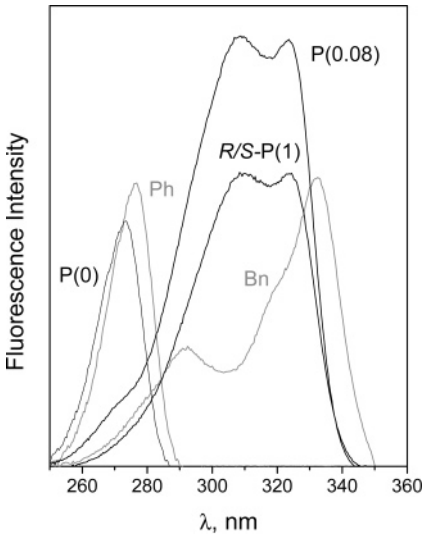

Figure 5. Uncorrected excitation spectra for dilute solutions of Ph and P(0) upon emission of 292 nm and Bn, *R*/*S*-P(1), and P(0.08) upon emission of 355 nm in DCE at 25 °C.

spectra nearly match those of the absorption spectra. Any of the excitation spectra for P(*x*) copolymers whatever the PhO content is, upon observation of PhO emission (292 nm), are shown in Figure 5 as no emission at all is observed when selecting this wavelength for any of these samples. This is another evidence of the highly efficient PhO → BnO transfer. Similar spectra were collected in DCE and NMP.

Fluorescence Quantum Yields. Quantum yields (ϕ_f) were obtained by the method described by us[30] using quinine sulfate in 0.1 M sulfuric acid as a standard. The bottom of Figure 6a depicts the variation in quantum yields for dilute solution Bn/Ph mixtures that have different molar fractions of BnO (*x*), under excitation of 270 and 325 nm in THF at 25 °C. Emission upon excitation of 325 nm only shows the band due to the emission of BnO. Upon excitation of 270 nm it exhibits a combination of bands due to the emission of both molecules which do not interact. The fluorescence quantum yields, at any excitation wavelength, are very low, and they stay nearly constant with *x*. ϕ_f for Bn and Ph model compounds in DCE and NMP reveal a slight dependence on the solvent nature, but they are also very low.

Table 1. ϕ_f and $\langle\tau\rangle$ (Bold) for Dilute Solution of Homopolymers P(1) in Different Solvents at the Temperature of 25 °C upon Excitation of 270 and 305 nm (in Parentheses); $\langle\tau\rangle$, in ns, Was Obtained at λ_{em} = 355 nm

homopolymer	DCE	THF	NMP
R/*S*-P(1)	0.06 (0.07)	0.10 (0.15)	0.03 (0.13)
	1.9 (1.8)	**2.4 (2.5)**	**2.7 (2.6)**
R-P(1)	0.06 (0.07)	0.07 (0.12)	0.03 (0.12)
	1.8 (1.1)	**2.3 (2.2)**	**2.8 (2.6)**
S-P(1)	0.09 (0.06)	0.08 (0.12)	0.03 (0.13)
	1.4 (1.1)	**2.3 (2.3)**	**2.4 (2.3)**

Figure 6a also depicts quantum yields for polymers as a function of *x* in THF at 25 °C. At any polymer composition, *x*, whatever the excitation wavelength the emission spectra only show a typical BnO band with a maximum centered around 355 nm. Obviously the exception is P(0). An increase in the fraction of BnO content means a monotonic decrease in the values of ϕ_f, which is patent for the first members of the series P(0)−P(0.42). Either P(0.70) and *R*/*S*-P(1) or P(0.42) deviates a little from this behavior. Fluorescence quantum yields show a slight dependence on the solvent nature, but as depicted in Figure 6b in DCE or NMP, they exhibit a similar variation with *x*. As shown in Table 1, optically active *R*- and *S*-P(1) homopolymers show the smallest quantum yields at both excitation wavelengths, but they are similar to the ones obtained for the racemic *R*/*S*-P(1) mixture in any of the solvents used.

Fluorescence Lifetime Measurements. Fluorescence intensity decays on THF dilute solutions of Ph or Bn upon excitation of 270 nm and under observation of their respective maximum emission bands (292 and 355 nm) are, as expected, monoexponentials with lifetimes of approximately 2.7 and 1.0 ns, respectively. The lifetime for Bn does not change appreciably from 1 ns when changing the excitation at 325 nm. Decays for Bn/Ph mixtures at 355 nm, when both chromophores are excited (270 nm), exhibit two components that are characteristic for isolated Ph and Bn of ∼3 and ∼1 ns, whose relative proportion decreases as the Bn content increases. When 325 nm is used as the excitation wavelength, results show that Ph is also slightly excited. Two components with values that are comparable to those for the individual Ph and Bn were also obtained. Nevertheless, the contribution of the fastest component due to Bn (∼1 ns) is larger than 97%, whatever the composition is.

Figure 7 depicts the values of $\langle\tau\rangle$ vs *x*, obtained from the analysis of individual lifetime components and preexponential factors by using eq 2 under observation of the BnO emission maximum band. Values of $\langle\tau\rangle$ placed in the lower part of the plot correspond to the Ph/Bn mixtures, which upon excitation of 270 nm initially seem to decrease slightly with *x*, i.e., as the mixture has a higher content of the chromophore with the fastest decay component, reaching a plateau for $x > 0.2$. Upon excitation at the wavelength of 325 nm, $\langle\tau\rangle$ values seem to be practically independent of *x*. Something similar occurred with the fluorescence quantum yields.

The fluorescence intensity decay profiles for dilute solution of P(*x*) were also obtained under observation of the BnO in THF and DCE at 25 °C. Decays for P(0) through P(0.42) in THF (or DCE), upon excitation of 270 or 305 nm, were reasonably fitted to a two-exponential function. Decay components (at 270 nm) for P(0)−P(0.42) are in the 1.9−2.8 and 8.1−3.0 ns ranges. The latter component becomes faster with *x*. In addition to these two components a third even faster lifetime component of ∼0.7−0.9 ns appears for P(0.70) and homopolymers *R*/*S*-P(1), *R*-P(1), or *S*-P(1), whereas the slowest one takes the values closer to the upper limit of the pointed range. When P(0)−P(0.42) are excited at 305 nm, the main differences are

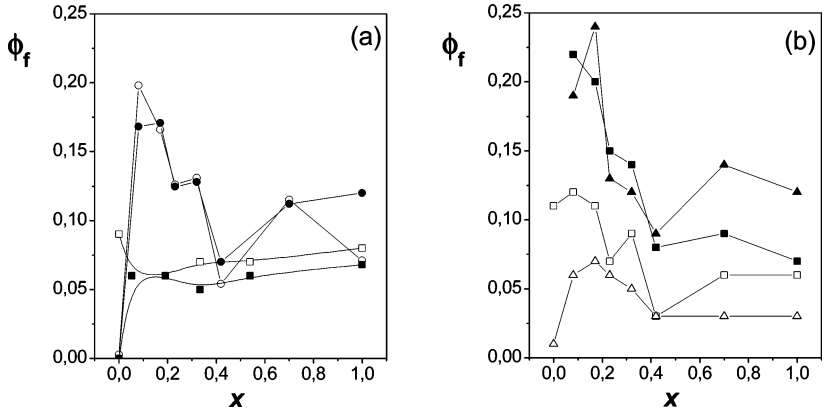

Figure 6. (a) Variation of fluorescence quantum yields with *x* for Bn/Ph dilute solution mixtures in THF at 25 °C with different molar fractions of BnO (*x*) under excitation of 270 nm (□) and 325 nm (■) and P(*x*) upon excitation of 270 nm (○) and 305 nm (●). (b) Idem for *P*(*x*) in DCE (squares) and NPM (triangles).

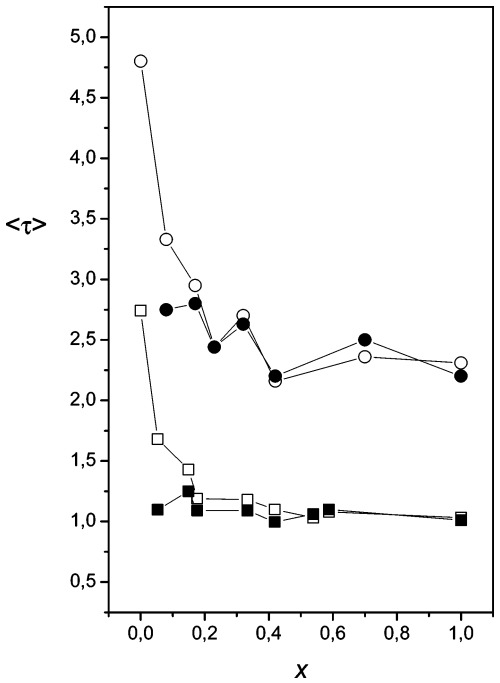

Figure 7. Change of the average lifetime $\langle\tau\rangle$ with *x* for Bn/Ph dilute solution mixtures in THF at 25 °C with different molar fractions of BnO (*x*) under excitation of 270 nm (□) and 325 nm (■) and P(*x*) upon excitation of 270 nm (○) and 305 nm (●) at the same experimental conditions. $\lambda_{em} = 355$ nm.

that the first component slightly decreases from the value obtained at 270 nm, and the second one remain always close to 3.0 ns. However, the aim of the present work is to obtain the dependence of $\langle\tau\rangle$ with the copolymer composition, *x*, and not to find the physical interpretation of the individual components of the decay.

Average lifetimes $\langle\tau\rangle$ for P(*x*), which are shown in the upper part of Figure 7, clearly decrease when increasing *x* for the first members of the series and especially upon excitation at 270 nm. The last two members of the series do not seem to change with the composition. This trend is less marked when the samples are excited at 305 nm. Similar behavior was described with fluorescence quantum yields in the previous section. Average lifetimes $\langle\tau\rangle$ for binaphthoxyphosphazene homopolymers in different solvents are also collected in Table 1. Results reveal that $\langle\tau\rangle$ values for the *S*-P(1) and *R*-P(1) optically active samples that contain helix fragments along the chain always of same screw direction are, in general, slightly smaller than for the racemic optically inactive *R*/*S*-P(1) and smaller that any of the copolymers studied.

Table 2. Relative Values of Overlapping Integral, *J*, and Fluorescence Quantum Yield Donor, ϕ_D, to the Values for the Naphthalene to Naphthalene (N → N) Transfer at 25 °C

D → A transfer	$J_{D\to A}/J_{N\to N}$	ϕ_D/ϕ_N	$R_{0,D\to A}$ (Å)
Bn (270 nm) → Bn	1.16	2.0	8.1 ± 0.4
Bn (325 nm) → Bn	1.16	1.65	7.8 ± 0.4
Ph (270 nm) → Ph	0.16	1.21	5.3 ± 0.2
Ph (270 nm) → Bn	7.96	1.21	10.2 ± 0.4

Förster Radii for the Intramolecular Energy Transfer. According to eq 4, the ratio of the R_0's for the transfer of two small donor molecules, D and D′, in dilute solution ($\kappa^2 = {}^2/_3$) under the same conditions can be written as

$$(R_{0,D\to A}/R_{0,D'\to A'})^6 = (\phi_D/\phi_{D'})(J_{D\to A}/J_{D'\to A'}) \qquad (6)$$

Using a standard whose value of $R_{0,D'-A'}$ is known as D′; any other R_0 can be estimated from the experimental ϕ and *J* obtained for both systems. As a standard we use naphthalene (N) for whose self-transfer Berlman reported values of $R_{0,N\to N}$ = 7.35 and 6.79 Å.[31,32] *J* was obtained by the graphical integration of eq 5. Measurements of ϕ and *J* for dilute solutions of N, Ph, and Bn in THF at 25 °C provide values of ϕ_D/ϕ_N and $J_{D\to A}/J_{N\to N}$ for the PhO → PhO, BnO → BnO, and PhO → BnO transfer which are collected in Table 2. The analysis gives R_0 for the BnO → BnO transfer of ∼8 Å at any of the wavelengths used, which is slightly larger than the N → N one. Much larger is the Förster radius for the PhO → BnO transfer (∼10 Å), whereas the value for PhO → PhO is smaller (∼5 Å).

Fluorescence Polarization Measurements. The left panel of Figure 8 depicts the excitation spectra for Bn, Ph, and *R*/*S*-P(1) superimposing the excitation anisotropy spectra for Bn and the P(*x*) series measured in DCE at 0 °C by monitoring the maximum of emission for BnO. The right panel shows the emission anisotropy spectra for Bn and P(*x*) upon excitation of 325 and 305 nm, respectively, and the emission spectra for Bn and *R*/*S*-P(1) under the same experimental conditions.

In the region of both emission and excitation spectra, where samples show enough intensity, systems nearly always have values of *r* that are smaller than 0.1. Bn, a system where energy transfer is absent at these experimental conditions, do not show largest values of *r* as usually occurs with other model compounds for polymers containing a single chromophore in a more rigid media.[33,34] Rotational diffusion of this small molecule is still present. However, the main feature of the results shown in

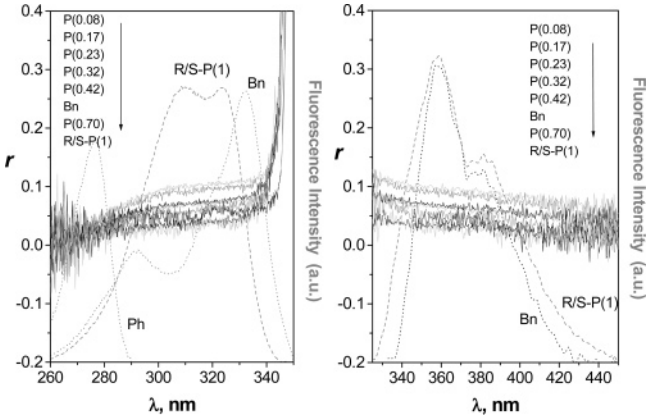

Figure 8. Left panel. Excitation anisotropy spectra for dilute solutions of Bn and the P(*x*) polymer series in DCE at 0 °C upon $\lambda_{em} = 355$ nm (emission for BnO). Superimposed are the uncorrected excitation spectra for Bn, Ph, and *R*/*S*-P(1) at the same experimental conditions. Right panel. Emission anisotropy spectra for Bn and P(*x*) under λ_{ex} of 325 and 305 nm, respectively. Overlapping are the uncorrected emission spectra for Bn and *R*/*S*-P(1) measured at the same experimental conditions.

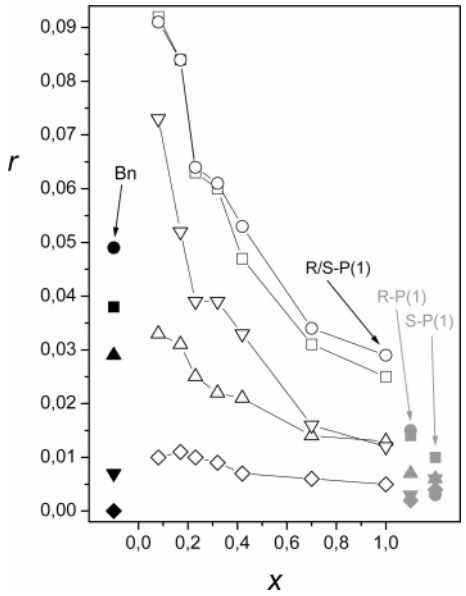

Figure 9. Anisotropies *r* vs *x* obtained from the excitation and emission anisotropy spectra at different excitation and emission wavelengths: (○) $\lambda_{exc} = 305$ nm, $\lambda_{em} = 340-410$ nm (0.010−0.006), (□) $\lambda_{exc} = 355$ nm, $\lambda_{em} = 280-330$ nm (0.016−0.009), and (◇) $\lambda_{exc} = 355$ nm, $\lambda_{em} = 265-285$ nm (0.025−0.012) in DCE at 0 °C. Values and standard deviation (in parentheses) in *r* were obtained from the averaged values in the wavelength range stated, which approximately corresponds to a bandwidth with limits that are half the height of the maximum band intensity. (▽) $\lambda_{exc} = 305$ nm, $\lambda_{em} = 355$ nm and (△) $\lambda_{exc} = 270$ nm, $\lambda_{em} = 355$ nm in THF at 0 °C, obtained at the excitation and emission wavelength selected by averaging five independent measurements. Filled gray symbols correspond to *R*-P(1) and *S*-P(1) and black ones to Bn at the same conditions.

both panels of Figure 8 is that *r* for P(*x*) exhibits a monotonic decrease with *x*.

Figure 9 depicts anisotropy changes with *x* for polymers at several pairs of excitation and emission wavelengths in DCE and THF at 0 °C. The anisotropy measured at the BnO emission always exhibits a monotonic decrease of *r* with *x* pointed out in the previous paragraph. For dilute solutions of polymers at low temperatures, where rotational diffusion and conformational change rates are diminished, a decreasing of the fluorescence anisotropy means an increase of intramolecular energy transfer.[15] These results denote an increase of energy transfer between BnO units as the content of this group increases in the copolymer.

When both PhO and BnO are excited (270 nm), there is chance of obtaining anisotropies for P(*x*) when monitoring PhO emission for any of the P(*x*). No emission is obtained from this group. When BnO emission is, however, focused, *r* values again decrease with increasing *x*, but the absolute values are smaller than those obtained when the BnO groups are directly excited. More transfer processes are involved, thus decreasing *r* values.

These results, together with those of fluorescence quantum yield and lifetimes, indicate that the energy transfer by resonance mechanism in P(*x*) may consist of a highly efficient (100%) PhO → BnO process followed by a BnO → BnO migration between binaphthoxyphosphazene units. This process is also accompanied by a decrease in BnO fluorescence quantum yields and lifetimes. As copolymers contain chlorine unsubstituted phosphazenes units these may perhaps act as traps for the energy migration. The former process does not depend on *x*. The efficiency of the latter as well as the BnO fluorescence quenching increases with the BnO content, which produces higher content of (left-handed) helical conformation fragments in the binaphthoxyphosphazene sequences.[4,5] On the other hand, anisotropies *r* for *R*-P(1) and *S*-P(1), shown in Figure 9, are smaller than for the racemic optically inactive *R*/*S*-P(1). Average lifetime and quantum yields values also suggest a similar behavior. These results may agree with the fact that BnO energy migration would be favored by an increase not only of the number and length of helix sequences but also by the presence of sequences of the same screw direction along the poly(binaphthoxyphosphazene) chain. The PhO → PhO transfer process, whose efficiency may, obviously, be smaller due to the lower R_0 cannot be disregarded.

Molecular Dynamics. The interactions considered for the transfer in $A_{10}-B-A_{10}$ fragments, F1−F4, were those that involve the chromophores of the central unit B and those from the five nearest repeating units placed at both sides (Figure 2), i.e., interaction between the aromatic groups of B and those for the two closest A neighbor units (I1), the two second neighboring ones (I2), the third neighboring ones (I3), and so on for I4 and I5. Interactions are schematized in Figure 2. Another five units at both ends were added to avoid end-chain effects. Three parameters related to the resonance energy transfer efficiency for the $A_{10}-B-A_{10}$ fragments (F1−F4) were calculated: (a) The probability, $P(R)$, of finding the center of mass[35] of each aromatic group pending of the unit A involved in the interaction within a sphere of radius *R* centered at the center of mass of each of the aromatic group attached to the central phosphazene units, B. This value can be obtained as

$$P(R) = \int_0^R w(R)\,\mathrm{d}R \tag{7}$$

where $w(R)$ is the distribution function of the distance between the centers of the aromatic groups involved. (b) The average of all the distances for each particular interaction $\langle R \rangle$ and orientational factor $\langle \kappa^2 \rangle$ for fixed dipole transition moments of absorption and emission along the C(9) and C(10) for BnO or C(1) and C(4) for PhO. (c) The efficiency in the intramolecular energy transfer obtained as

$$\Phi_{RET} = \left\langle \left(1 + \frac{(2/3)R^6}{\kappa^2 R_0^{\,6}} \right)^{-1} \right\rangle \tag{8}$$

The averages take into account all possible chromophore interactions for the fragments studied. Experimental values were

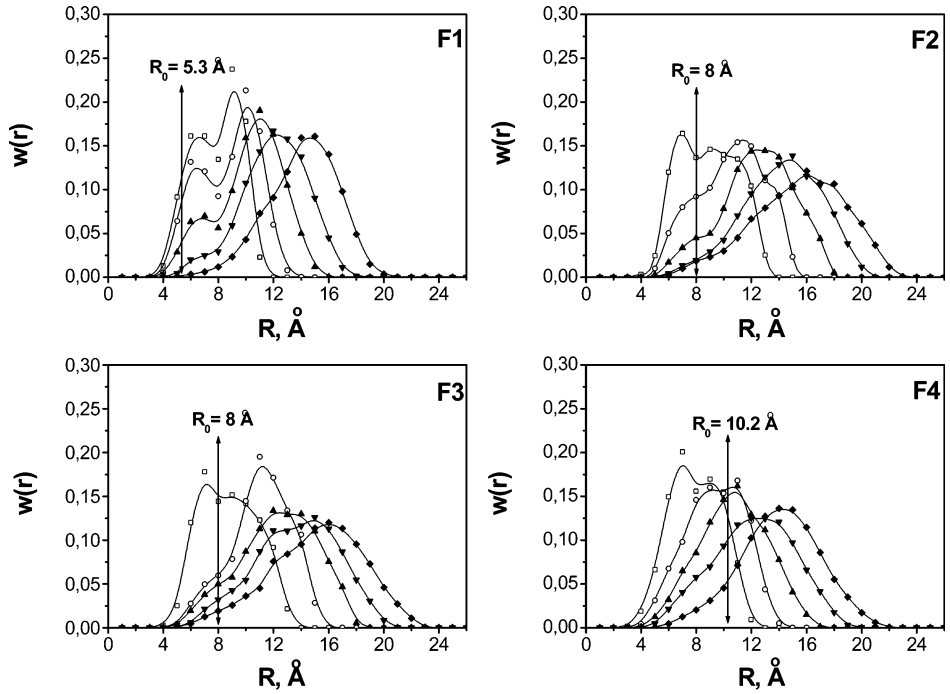

Figure 10. Average of the distribution of the distances between the chromophores of the central phosphazene B unit and those for A, the nearest-neighboring unit I1 (○), the second neighboring one I2, (□), the third I3 (▲), chromophores for the fourth unit I4 (▼), and the fifth one I5 (◆) for the different fragments studied, F1, F2, F3, and F4, obtained from the analysis of MD trajectories.

Table 3. Average of Several Parameters Related to the Efficiency of Energy-Transfer Processes for the Fragments F1−F4 and Different Interactions Denoted by I1−I5 Obtained from the Analysis of MD Trajectories at 1000 K; in Parentheses Are the Parameters for the Helix Conformations for F2 and F3 Which Simulate the Optically Active *R*-(−)-[NP($O_2C_{20}H_{12}$]$_n$ and *S*-(+)-[NP($O_2C_{20}H_{12}$)]$_n$ Polyphosphazenes, Respectively

	$\langle R\rangle$ (Å)	$\langle\kappa^2\rangle$	$P(R_0)$	Φ_{RET}
F1				
I1	7.4	0.96	0.15	0.18
I2	8.2	0.61	0.10	0.10
I3	9.8	0.49	0.05	0.05
I4	11.5	0.47	0.00	0.02
I5	13.6	0.49	0.00	0.01
F2				
I1	8.3 (11.1)	0.47 (0.59)	0.45 (0)	0.34 (0.11)
I2	10.0 (5.7)	0.57 (0.61)	0.23 (1)	0.23 (0.73)
I3	11.9 (12.3)	0.64 (0.93)	0.10 (0)	0.14 (0.12)
I4	13.7 (10.1)	0.62 (0.41)	0.04 (0)	0.08 (0.14)
I5	14.9 (14.9)	0.69 (1.19)	0.03 (0)	0.07 (006)
F3				
I1	8.3 (10.8)	0.48 (0.57)	0.47 (0)	0.35 (0.13)
I2	10.5 (5.5)	0.49 (0.63)	0.14 (1)	0.17 (0.72)
I3	11.8 (12.3)	0.65 (0.88)	0.11 (0)	0.15 (0.12)
I4	13.1 (9.6)	0.71 (0.51)	0.06 (0)	0.11 (0.22)
I5	14.6 (14.8)	0.69 (1.23)	0.04 (0)	0.07 (0.06)
F4				
I1	7.5	0.50	0.94	0.65
I2	8.9	0.51	0.70	0.49
I3	10.2	0.56	0.49	0.39
I4	11.7	0.61	0.31	0.29
I5	13.5	0.63	0.13	0.18

assigned for R_0. Figure 10 depicts the distribution function for the average of distances between the chromophores involved in each I1−I5 interaction for the four structures, F1−F4, studied. Results for all of the fragments, as expected, show a shift of the maximum of each distribution to larger distances when going from I1 to I5. The second column of Table 3 collects $\langle R\rangle$ for each particular interaction and fragment. These values obviously increase when increasing the separation between interacting groups. Most of the $\langle\kappa^2\rangle$ values, which are included in the third column, are slightly smaller than those expected ($\kappa^2 = {}^2/_3$) for

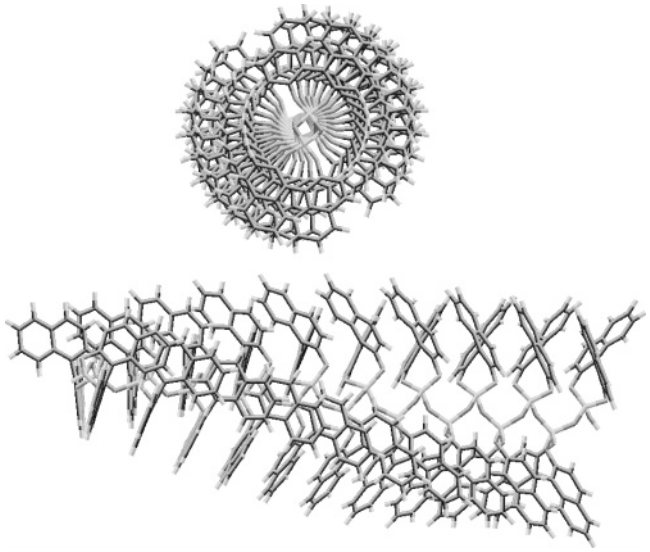

Figure 11. Front and side views of a right-handed helix conformation for a *S*-(+)-[NP($O_2C_{20}H_{12}$)]$_n$ chain containing 10 repeating units. Notice BnO interaction between odd (and even) phosphazene units.

chromophores that move fast and whose transition dipoles moments randomize prior to transfer. Table 3 also shows the probability $P(R)$ for $R = R_0$, which corresponds to the area under the curves of the plots depicted in Figure 11 for $R \le R_0$. The simple observation of this parameter infers that I1 and I2 interactions, especially the first one, are mostly responsible for energy transfer between PhO for F1 with a probability larger than 0.1 or between the BnO ones for F2 and F3, with also a contribution of I3. All interactions seem to contribute to the high efficiency of the PhO → BnO process that takes place for F4 with a probability always higher than 0.13.

The efficiency of the processes obtained by using eq 8 is also collected in the last column of Table 3. Results show patterns that are similar to those obtained from $P(R)$. PhO mainly transfers energy to a PhO group from the neighboring phos-

phazene units with an efficiency of 0.18, but also to the nearest-neighboring ones with an efficiency of 0.10. *R*- and *S*-BnO mainly transfer their excitation energy to the BnO attached to the neighboring phosphazene unit with a high efficiency (∼0.35). But they can also transfer it to BnO groups placed farther away. The PhO → BnO process, however, can even take place with very high efficiency between chromophores placed five phosphazenes units away. Another parameter calculated, not included in Table 3, was the probability of finding at least one interaction that fulfills the same requirements as $P(R)$ for each conformation; i.e., at least one pair of chromophores, regardless of their separation along the chain, have their respective centers of masses at a distance equal to or smaller than R_0. The results, quite significantly, are 0.28, 065, 0.63, and 0.99 for the fragments F1 to F4, respectively.

Table 3 also contains, in parentheses, the parameters for the initial helix conformations of F2 and F3, which correspond to the optically active *R*-(−)- and *S*-(+)-$[NP(O_2C_{20}H_{12})]_n$ polyphosphazenes. $\langle R \rangle$, which is obtained from the average of the chromophore distances for the single helix conformation, clearly shows an odd−even effect with the minimum value for I2, the only one which is smaller than R_0 (8 Å). The helix conformation for F2 and F3 fragments are left- and right-handed, respectively, and with this arrangement, each BnO is superimposed by another BnO pending from the next to nearest-neighbor phosphazenes units, as Figure 10 depicts. Results point to I2 as the most favorable interaction for the energy transfer. $\langle \kappa^2 \rangle$ does not show any special trend, and it does not provide the larger value for I2 either. However, Φ_{RET} again gives values that are much larger (>0.7) for this particular interaction than for any other.

These results infer that the energy transfer for the helix conformation fragments is highly efficient, and it apparently takes place by interaction between BnO from odd (and even) phosphazenes units. These theoretical results are also in agreement with the experimental ones showing that the presence of helical sequence fragments (preferably in the same chirality), which are favored by increasing the BnO content in the copolymer,[4,5] may increase migration energy efficiency between them. The effect grows with increasing length of the helical sequences.

Conclusions

From the experimental point of view, emission and excitation spectra, fluorescence quantum yield, fluorescence lifetime, and fluorescence depolarization measurements on dilute solution of *R*-(−)-, *S*-(+)-, and optically inactive *R*/*S*-$[NP(O_2C_{20}H_{12})]_n$ homopolymers as well as six random copolymers $\{[NP(O_2C_{20}H_{12})]_x[NP(OC_6H_5)_2]_{1-x}\}_n$ with a different composition x in dilute solution of several solvents were performed. Some fragments of these polymers were also simulated employing MD procedures. Theoretical values of the parameters related to the efficiency of energy transfer obtained from the analysis of MD trajectories agree with a 100% efficiency for the PhO → BnO process, which does not depend on x, followed by a highly efficient energy migration between BnO which increases with x. Theoretical results are in agreement with experimental values of fluorescence anisotropy, which suggests that the latter process may be favored by the presence of helix conformation sequences of the same chirality along the poly(binaphthoxyphosphazene) chain. The whole process is followed by a decrease in the fluorescence properties of BnO. On the other hand, the agreement between theoretical and experimental results provides strong evidence for the presence of helical segments involving binaphthoxyphosphazene units in these polymers. The number and length of such segments seems to increase with the BnO content as was inferred in previous works. Thus, the existence of these helical segments, which is clearly shown in the DM simulations, explains the fluorescence behavior of these systems. Moreover, they also provide a reasonable explanation for some other conformational properties such as the high values of the unperturbed dimensions.

Acknowledgment. This research was supported by DGICYT (Projects BQU2001-1158, CTQ2004-01484-BQU, and CTQ2054-04710-BQU) and CAM (GR/MAT/0810/2004). We acknowledge the assistance of M. L. Heijnen with the preparation of the manuscript.

References and Notes

(1) De Jaeger, R.; Gleria, M. *Phosphazenes. A Worldwide Insight*; Nova Science: New York, 2004.
(2) Allcock, H. R. *Chemistry and Applications of Polyphosphazenes*; Wiley and Sons: New York, 2002.
(3) Mark, J. E.; Allcock. H. R.; West, R. *Inorganic Polymers*; Prentice Hall: Englewood Cliffs, NJ, 1992.
(4) Carriedo, G. A.; García Alonso, F. J.; González, P. A.; García Alvarez, J. L. *Macromolecules* **1998**, *31*, 3189−3196.
(5) Carriedo, G. A.; García Alonso, F. J.; Gómez Elipe, P.; García Alvarez, J. L.; Tarazona, M. P.; Rodríguez Laguna, M. T.; Saiz, E.; Vázquez, J. T.; Padrón, J. I. *Macromolecules* **2000**, *33*, 3671−3679.
(6) Rodríguez Laguna, M. T.; Tarazona, M. P.; Carriedo, G. A.; García Alonso, F. J.; Hidalgo, J. I.; Saiz, E. *Macromolecules* **2002**, *35*, 7505−7515.
(7) Carriedo, G. A.; García Alonso, F. J.; Lombardo, G. M.; Pappalardo, G. C.; Punzo, F. *Chem.−Eur. J.* **2004**, *10*, 3775−3782.
(8) Carriedo, G. A.; García Alvarez, J. L.; García Alonso, F. J.; Presa, A.; Tarazona, M. P.; Mendicuti, F.; Marcelo, G. *Macromolecules* **2004**, *37*, 5437−5443.
(9) Förster, Th. *Ann. Phys.* **1948**, *6*, 55−75.
(10) Bravo, J.; Mendicuti, F.; Saiz, E.; Mattice, W. L. *Macromol. Chem. Phys.* **1994**, *195*, 3411−3424.
(11) Bravo, J.; Mendicuti, F.; Saiz, E.; Mattice, W. L. *Macromol. Chem. Phys.* **1996**, *197*, 1349−1360.
(12) Haile, J. M. *Molecular Dynamics Simulations: Elementary Methods*; John Wiley & Sons: New York, 1992.
(13) Allen, M. P.; Tildesley, D. J. *Computer Simulation of Liquids*; Clarendon Press: Oxford, 1987.
(14) O'Connor, D. V.; Ware, W. R.; André, J. C. *J. Phys. Chem.* **1979**, *83*, 1333−1343.
(15) Lakowicz, J. R. *Principles of Fluorescence Spectroscopy*, 2nd ed.; Kluwer Academic/Plenum: New York, 1999; Chapter 10.
(16) Guillet, J. *Polymer Photophysics and Photochemistry*; Cambridge University Press: Cambridge, 1985.
(17) Phillips, D. *Polymer Photophysics: Luminescence, Energy Migration and Molecular Motion in Synthetic Polymers*; Chapman and Hall: New York, 1985.
(18) Rabek, J. F. *Mechanism of Photophysical Processes and Photochemical Reactions in Polymers: Theory and Applications*; John Wiley & Sons: Chichester, 1987.
(19) Forester, T. R.; Smith, W. *DL_POLY (Version 2.10)*; Daresbury: Warrington WA4 4AD; Daresbury Laboratory, England; http://www.cse.clrc.ac.uk/msi/software/DL_POLY/.
(20) http://www.amber.ucsf.edu/amber/amber.html, http://www.amber.ucsf.edu/amber/dbase.html, http://pharmacy.man.ac.uk/amber/.
(21) Tarazona, M. P.; Saiz, E. *Polymer* **2000**, *41*, 3337−3347.
(22) Rodriguez Laguna, M. T.; Saiz, E.; Tarazona, M. P. *Polymer* **2000**, *41*, 7993−8000.
(23) Sybyl 6.9, Tripos Associates, St. Louis, MO.
(24) Gasteiger, G.; Marsili, M. *Tetrahedron* **1980**, *36*, 3219−3228.
(25) Streitwieser, M. *Molecular orbital Theory for Organics Chemists*; Wiley: New York, 1961.
(26) Brunel, Y.; Faucher, H.; Gagnaire, D.; Rasat, A. *Tetrahedron* **1975**, *31*, 1075−1091.
(27) Press, W. H.; Flannery, B. P.; Teukolski, S. A.; Vetterling, W. T. *Numerical Recipes: The Art of Scientific Computing*; Cambridge University Press: Cambridge, 1988; p 312.
(28) Hargreaves, J. S.; Webber, S. E. *Polym. Photochem.* **1982**, *2*, 359−366.
(29) Cione, A. P.; Scaiano, J. C.; Neumann, M. G.; Gessner, F. *J. Photochem. Photobiol.* **1998**, *118*, 205−209.

(30) Mendicuti, F.; Mattice, W. L. *Polym. Bull. (Berlin)* **1989**, *22*, 557−563.
(31) Berlman, I. B. *Handbook of Fluorescence Spectra of Aromatic Molecules*; Academic Press: New York, 1971; p 421.
(32) Berlman, I. B. *Energy Transfer Parameters of Organic Compounds*; Academic Press: New York, 1973; p 308.
(33) Mendicuti, F.; Saiz, E.; Mattice, W. L. *Polymer* **1992**, *33*, 4908−4912.
(34) Gallego, J.; Mendicuti, F.; Saiz, E.; Mattice, W. L. *Polymer* **1993**, *34*, 2475−2480.

(35) The center of masses of phenyl rings were assumed to be the middle point of the virtual bond connecting C(1) and C(4) of the ring. In the case of naphthoxy groups, the middle point of the actual C(9)−C(10) bond were taken as center of masses of the group. Thus, eight distances were computed for each kind of interaction, i.e., two groups in the central B unit with two groups in each of the two corresponding A units.

MA052063D